An improved position reconstruction method for radioactive particle tracking

Ghazaleh Mirakhori[a,b], Audrey Collard-Daigneault[a], Amishga Alphonius[a], Jocelyn Doucet[c], Bruno Blais[a], Jamal Chaouki[b,*]

[a]*Research Unit for Industrial Flows Processes (URPEI), Department of Chemical Engineering, Polytechnique Montréal, PO Box 6079, Stn Centre-Ville, Montréal, QC, Canada, H3C 3A7*
[b]*Process Engineering Advanced Research Lab (PEARL), Department of Chemical Engineering, Polytechique Montréal, PO Box 6079, Stn Centre-Ville, Montréal, QC, Canada H3C 3A7*
[c]*Pyrowave Inc, Montréal, QC, Canada H2N 2B7*

Abstract

This work introduces a novel reconstruction method exploiting the inverse of Finite Element Method (FEM) to reconstruct positions from ray tracing experimental measurement such as those obtained by radioactive particle tracking. FEM based Position Reconstruction (FEM-PR) relies on shape function evaluation within simplex elements (i.a tetrahedron) for position reconstruction using a mean-square problem, which has proven to be robust, accurate, and fast. Tracer positions are reconstructed under the condition that least-squares compatibility is maintained between experimental counts and interpolated values within inverse elements. This approach is implemented in a module within the open-source software, Lethe-RPT, enabling user to carry out radioactive particle tracking (RPT) experiments from calibration to tracer position reconstruction. The test benchmark and experimental setup are described. For the same test cases, the reconstruction error is investigated using an increasing number of inverse elements and Monte Carlo (MC) iterations. The accuracy and robustness of FEM-PR concerning the inevitable measurement errors due to calibration, measurement systems, and the quantized nature of γ-rays is demonstrated. This approach provides a new view for immediate and precise position reconstruction. FEM-PR reconstructs the tracer position

*Corresponding author
Email address: jamal.chaouki@polymtl.ca (Jamal Chaouki)

with an accuracy of 0.08 mm. Approximately 3.37 ms is required to reconstruct one position on a desktop computer, which is less than the sampling time for experimental data collection.
Keywords: Radioactive Particle Tracking (RPT), Finite Element Method (FEM), Monte Carlo methods, Reconstruction algorithm, Non-invasive technique

1. Introduction

Developing a reliable experimental approach for designing chemical reactors is one of the key challenges in multiphase flow reactor engineering. Scaling up chemical reactors requires a reliable description of the hydrodynamics. The inability to properly describe the flow patterns will inevitably lead to poor performance of scaled-up reactors [1, 2, 3]. To address this need, several experimental techniques have been developed to study the dynamics of multiphase flows. These techniques are categorized as intrusive and non-intrusive methods. As the name suggests, intrusive methods measure fluid velocity by interacting with the fluid. Such methods include Pitot tube, Hot Wire Anemometry (HWA), and optical probes. Non-intrusive techniques characterize the flow without disturbing the flow. Laser Doppler Anemometry (LDA), Particle Image Velocimetry (PIV), Positron Emission Particle Tracking (PEPT), Magnetic Resonance Imaging (MRI), and Radioactive Particle Tracking (RPT) are examples of non-intrusive techniques [4].

Unlike other non-intrusive methods, RPT copes well with opaque systems [5]. Other methods which use light or laser fail in systems with a large volume fraction of the dispersed phase. Due to the extensive demands of RPT for computational resources, researchers use this technique offline. It is nevertheless desirable to monitor the hydrodynamics of pilot scale and industrial reactors in real time with high accuracy [6, 7, 2].

The objective of this paper is to present a highly accurate and noise-insensitive method that would apply to any domain geometry and experimental configuration. To accomplish this, our work presents a novel particle position reconstruction algorithm called FEM-PR. This technique follows

the principle of the inverse Finite Element Method. The inverse problem of FEM was first introduced to enable real-time tracking of the three-dimensional displacement field of a structure, often called shape sensing. iFEM reconstructs structural deformations using experimental strains and minimizing a weighted least-squares function [8]. The FEM-PR method, also derived from the inverse problem of FEM, can monitor the dynamics of a multiphase flow system in real-time. FEM-PR uses the experimental data of photon counts received from a radioactive particle and solves a least-squares function between experimental and numerical values. The implementation of this technique makes RPT method more practical for industrial applications and accelerates research and development of more advanced reactors. This novel position reconstruction strategy has been implemented in Lethe-RPT, a module of Lethe [9], an open-source Computational Fluid Dynamics (CFD) library. We also present the implementation of the NOMAD blackbox optimizer to proceed with the model parameter tuning of the RPT experiments. Blackbox optimizer overcomes the Monte Carlo model's stochastic nature, and it obtains a precise set of unknown parameters for each detector from the calibration data.

In the following sections, we will introduce the mathematical framework of the RPT. Then, we present a derivative-free, blackbox optimizer that implements the Mesh-Adaptive Direct Search (MADS) algorithm for tuning the model parameters. Afterward, we introduce the FEM-PR approach. Finally, using benchmark cases and experimental validation, we demonstrate the capability and accuracy of the proposed algorithms for tracer position reconstruction.

2. Methodology

2.1. Monte Carlo model for photon counts calculation

RPT aims to reconstruct the motion of a radioactive particle by capturing the γ-rays it irradiates. Each RPT experiment includes the following steps: calibration, experiments, and position reconstruction [5].

A phenomenological model proposed by Beam *et al.* [10] associates the tracer position and the received photon count by a given detector as:

$$C = \frac{T\upsilon R\phi\xi(\overrightarrow{X})}{1 + \tau\upsilon R\phi\xi(\overrightarrow{X})} \tag{1}$$

where T is the sampling time (in seconds), ν is the number of γ-rays emitted by each disintegration, R is the activity of the tracer (in Beq), ϕ is the peak-to-total (photo peak) ratio, τ is the dead time of the detector (in seconds) per accepted pulse, and $\xi(\overrightarrow{X})$ is the efficiency of the detector associated with the tracer position which can be expressed as [10]:

$$\xi(\overrightarrow{X}) = \oiint_{\Omega} \frac{\overrightarrow{r}\,\mathrm{d}\overrightarrow{A}}{\|\overrightarrow{r}\|^3} f_a(\alpha,\theta) f_d(\alpha,\theta) \tag{2}$$

where, $\overrightarrow{r}$ is a vector from the position of the tracer to a point which γ-rays enter to the detector, $\mathrm{d}\overrightarrow{A}$ is the external surface vector normal to the surface at the contact point on the detector crystal, and Ω is the solid angle subtended by the radiation. Since there is no analytical solution to calculate the efficiency (except for some simple problems), a numerical method based on the Monte Carlo technique can compute Equation (2) [11]. This method generates thousands of random photon path directions towards a detector to estimate the surface integral of Equation (2). Beam *et al.* employed the Monte Carlo technique, which estimates this equation as:

$$\xi(X) = \frac{1}{N}\sum_{i=1}^{N} \omega_i f_a(\alpha,\theta) f_d(\alpha,\theta) \tag{3}$$

where N is the number of generated photon paths, the angles α and θ specify the direction of each traced ray from the tracer position, ω_i determines the solid angle for the particular selection of α and θ, and $f_a(\alpha,\theta)$ and $f_d(\alpha,\theta)$ are:

- f_a is the probability of non-interaction between the γ-rays emitted within Ω and the material inside the column:

$$f_a(\alpha, \theta) = \exp(-\mu_r e(\alpha, \theta)) \tag{4}$$

- f_d is the probability function of the γ-rays interaction with the detector:

$$f_d(\alpha, \theta) = 1 - \exp(-\mu_d d(\alpha, \theta)) \tag{5}$$

In Equation (4), μ_r is the total linear attenuation coefficient of the medium inside the reactor and $e(\alpha, \theta)$ is the length of the path travelled by a photon inside the reactor. In Equation (5), μ_d is the total linear attenuation coefficient of the detector, and $d(\alpha, \theta)$ is the effective distance travelled by γ-ray inside the crystal along the direction of α and θ angles [10].

However, some parameters of this model, such as the detector's dead time, source strength, and the medium attenuation coefficient, which is a parameter involved in calculating the efficiency, are unknown and unique to each experimental system.

The calibration phase plays a central role in finding the model unknowns. During the calibration procedure, the tracer is placed at many known positions inside the domain. The RPT system hardware records the γ-rays for a specified time to reach acceptable counting statistics at each position. The calibration process generates a 3D map of the photon counts received by each detector from the static positions. Finally, a parameter tuning algorithm compares the counts from the experimental measurement and the obtained counts from the Monte Carlo algorithm to find the model's unknown parameters. The algorithm obtains these unknowns by finding the optimum value of the Equation (6).

$$\min \sum_{i=1}^{N} \left(\frac{C_i - M_i}{C_i + M_i} \right)^2 \tag{6}$$

Where N is the number of sampling points, C is the calculated counts and M is the measured counts.

At the final step, a reconstruction algorithm converts the recorded photon counts to the instantaneous tracer positions. Over the past two decades, researchers have developed various techniques for more immediate and accurate position reconstruction, including the least-squares search algorithm, real coded genetic algorithm, and machine-learning algorithms [12, 7, 13, 2]. Support Vector Regression (SVR) was the most adequate technique among the proposed ones. Based on the experimental validation, this algorithm's Mean Absolute Error (MAE) was 1.45, 1.41, and 2.66 mm in the x, y, and z coordinates, respectively [2].

2.2. Phenomenological model parameter optimization using MADS

2.2.1. Description

Obtaining the parameters of the phenomenological model (see Eq. 1) using gradient-based optimization is difficult. The stochastic nature of the Monte Carlo model makes the calculation of the derivatives of error between the model-predicted counts and the experimental counts challenging. Therefore gradient-based optimization methods become rapidly ineffective. Due to all the limitations and complexity of implementation of the existing optimization methods, we propose to combine MADS, a non-gradient-based direct search optimization algorithm with the Monte Carlo technique to optimize the objective function. We achieved this by combining the NOMAD blackbox optimizer, which is a C++ implementation of the MADS algorithm, [14, 15] into the open source Lethe-RPT code.

This class of algorithms includes three steps: search, poll, and update. To begin the process, the algorithm determines an initial mesh M_0 of size Δ_0^m which represents a discretization of the solu-

tion domain. The MADS algorithm uses an initial point at each iteration to calculate the objective function at a finite number of points and put away the infeasible points. MADS compares the objective function values at feasible trial points with the current best possible value that it has found for the objective function so far. Each of the trial points lies on the current mesh with size Δ_k^m. By finding an improved mesh point the algorithm stops the iteration and the next iteration would start with a new incumbent solution $x_{k+1} \in \Omega$ with $f_\Omega(x_{k+1}) < f_\Omega(x_k)$. If the search algorithm fails to find a mesh point that decreases the objective function it calls for the poll step. At this step MADS evaluate the objective function at neighboring trial points which exist on a frame P_k with larger or equal size Δ_k^P from the previous mesh $\Delta_k^m \leqslant \Delta_k^P$. At the end, if both search and poll steps fail to find a better solution, the algorithm would decrease the mesh size and redo the first step using the current incumbent solution x_k. If either the search step or the poll step becomes successful, the algorithm will increase the mesh size and perform step 1 with the new incumbent solution x_{k+1} [16, 17, 15]. In the next section we discuss the integration of MADS algorithm with Lethe-RPT to optimize the detector's parameters.

2.2.2. Implementation in Lethe-RPT software

To start the optimization, NOMAD receives the input variables and their constraints presented in Table 1.

Table 1: Input, output and constraints for optimization of detector parameters

Input variables	Output Variables	Constraints
Position of the detector face center	Tracer activity	Tracer activity> 0
Position of a point on the detector axis	Detector dead time	Detector dead time> 0
Position of the calibration points	μ_r	$\mu_r > 0$
Experimental photon counts at calibration points	-	-
Initial guess for unknown variables	-	-

Prior to the optimization we set the parameters for the detectors (i.e., the photopeak-to-total ratio), the source (the crystal's attenuation coefficient, the number of γ-rays emitted), and the experimental

parameter (i.e., the sampling period) as well as those for optimization algorithm (e.g., optimization constraints and the maximum number of evaluation). To evaluate the objective function (Equation (6) at each step), NOMAD uses the parameters from the previous optimization step and it recalculates the counts implementing the Monte Carlo code. The algorithm stops once it reaches the maximum number of iterations. Figure 1 shows the algorithm of the parameter tuning process.

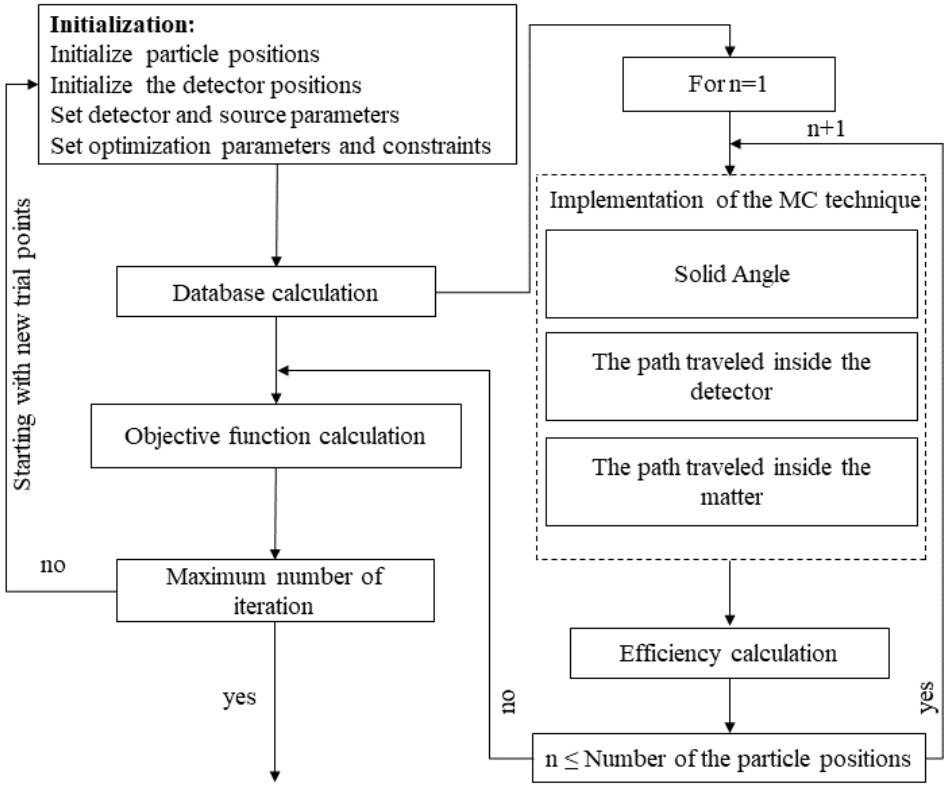

Figure 1: Optimization strategy algorithm

2.3. FEM-PR for back calculating the tracer position

2.3.1. Position reconstruction algorithm

First, FEM-PR filters the noise resulting from the Monte Carlo model by using an $\mathcal{L}^2$ orthogonal projection of the Monte Carlo model onto the domain. Then, the algorithm searches through the

cells and it minimizes the least-squares error between the photon count obtained from the FEM interpolation and the experimental count for all the detectors in each cell. Only the cell that satisfies the inverse of the finite element interpolation contains the tracer position. This novel approach uses the information from the previous position of the tracer and searches locally within the space around the last found position.

The first step in approximating a property using the finite element method is to build up a mesh over the domain of interest. Therefore, the 3D domain is discretized using linear tetrahedral elements. In the case of continuous approximations, isoparametric formulations can be used to approximate physical properties. Isoparametric elements are defined using natural and global coordinates. Each element's domain is mapped onto the global coordinate system using the shape functions constructed on its reference element. Therefore, an approximation of the physical values inside an element can be written in terms of shape functions and natural coordinates as:

$$\varphi_{x,y,z} = \sum_{i=1}^{n} N_i \varphi_i \tag{7}$$

where φ is a continuous physical value, $\varphi_{(x,y,z)}$ is the value at the global coordinate point (x, y, z), φ_i are the values at the nodes of the element and n is the number of nodes of the element ($n = 4$ for a linear tetrahedral element), and N_i are the shape functions defined as follows [18]:

$$N_1 = 1 - \eta - \xi - \zeta, \quad N_2 = \eta, \quad N_3 = \xi, \quad N_4 = \zeta \tag{8}$$

In case of RPT, the isoparametric approximation combined with a search algorithm can calculate the tracer's position using a set of photon counts received at each detector. The search algorithm

goes through each cell inside the domain and solves a least-squares cost-function defined as the difference between experimental and numerical values:

$$F = \sum_{i=1}^{N_D} (C_{num}^i - C_{exp}^i)^2 \tag{9}$$

where C_{num} and C_{exp} are the numerical and experimental counts, respectively, N_D is the number of detectors, and i is the number associated with the detector. The main search hypothesis is that the tracer is located inside the search element. The numerical count value within the finite element framework can be calculated using the isoparametric approximation previously presented:

$$C_{num} = \sum_{i=1}^{4} N_i C_i \tag{10}$$

The minimization of the least-squares function can be written by setting its partial derivatives to zero, which in vector-form results in:

$$F^{'} = \begin{bmatrix} F_1 \\ F_2 \\ F_3 \end{bmatrix} = \begin{bmatrix} \frac{\partial F}{\partial \eta} \\ \frac{\partial F}{\partial \xi} \\ \frac{\partial F}{\partial \zeta} \end{bmatrix} = \begin{bmatrix} 0 \\ 0 \\ 0 \end{bmatrix} \tag{11}$$

Since the elements are linear, this problem can be solved using the following system of equation:

$$\begin{bmatrix} \frac{\partial F_1}{\partial \eta} & \frac{\partial F_1}{\partial \xi} & \frac{\partial F_1}{\partial \zeta} \\ \frac{\partial F_2}{\partial \eta} & \frac{\partial F_2}{\partial \xi} & \frac{\partial F_2}{\partial \zeta} \\ \frac{\partial F_3}{\partial \eta} & \frac{\partial F_3}{\partial \xi} & \frac{\partial F_3}{\partial \zeta} \end{bmatrix} \begin{bmatrix} \eta \\ \xi \\ \zeta \end{bmatrix} = -F^{'} \tag{12}$$

where the matrix corresponds to the Jacobian of the element. Solving this system of equations, the

values of natural coordinates can be obtained. To decide whether the current parent cell can be considered as an appropriate cell for the particle position, the following conditions are checked and both need to be satisfied:

(a) $\eta, \zeta, \xi \in [0, 1]$

(b) $1 - \eta - \zeta - \xi \in [0, 1]$

Afterwards, the shape functions on the reference element are used to map the tracer position to the global coordinate system, $\mathbf{x}$:

$$\mathbf{x} = N(\varepsilon)\widetilde{\mathbf{x}} \tag{13}$$

where $N(\varepsilon)$ denotes a matrix composed of the shape functions, and $\widetilde{\mathbf{x}}$ corresponds to position in natural coordinates.

2.3.2. $\mathcal{L}^2$ orthogonal projection of the Monte Carlo model

Photon counts fluctuate in space due to the stochastic nature of the Monte Carlo technique, which can mislead the algorithm in position reconstruction. The algorithm uses the photon counts at the nodes of each element; therefore, the estimate of the tracer's position may be inaccurate if the nodal values are offset. Thus, rather than directly calculating photon counts at the nodes using the beam model, we approximate the value of photon counts at the nodes of the mesh by finding the coefficients c_j which minimize the following equation [19]:

$$\min_{c \in \mathbb{R}} ||f_i - \sum_j c_j \varphi_j|| \tag{14}$$

where c_j is the nodal photon counts and f_j is the photon counts calculated using the beam model (see Eq. 1). Finding the value of c_j is done by assembling and solving the following finite element system in the domain Ω:

$$\sum_j \int_\Omega \varphi_i c_j \varphi_j d\Omega = \int_\Omega \varphi_i f_i d\Omega \tag{15}$$

Through the solution of this system of equations, we can filter the oscillation of photon counts and have smooth photo counts as a function of position in space.

3. Results and discussion

3.1. Model parameter optimization using MADS

The case-study we use to validate our approach is a two-dimensional rectangular geometry having a $0.22\,\mathrm{m}$ length and $0.16\,\mathrm{m}$ width, and 0.02×0.02 m square mesh size (108 points). Figures 2a and 2b represent the experimental setup for the RPT tests and the configuration of the two-dimensional geometry, respectively. First, we evaluated the proposed optimization strategy using a simple case of one-dimensional tracer placement towards the detector. Next, we evaluated the algorithm implementing a two-dimensional arrangement of tracer placement. All the parameters used to obtain the results presented in this section are shown in Table 2.

Table 2: Parameters for optimization strategy

Parameter	Value
Source	Scandium-46
Number of γ-rays (ν)	2
Total linear attenuation coefficient of crystal (μ_d)	$2.477\,\mathrm{m}^{-1}$
Photopeak-to-total-ratio (ϕ)	0.4
Detector's crystal type	Sodium iodide (NaI)
Crystal length	$7.62\,\mathrm{cm}$
Crystal diameter	$7.62\,\mathrm{cm}$
Sampling-time (τ)	$1\,\mathrm{s}$

The detector saturation test inspired the one-dimensional validation approach. In this test, the radioactive tracer is moved along a line perpendicular to the detector's face. The detector is placed at a distance of $0.26\,\mathrm{m}$ from the center of the geometry. This test clarifies the space in which the detector cannot sense the actual radiation, called the blind zone.

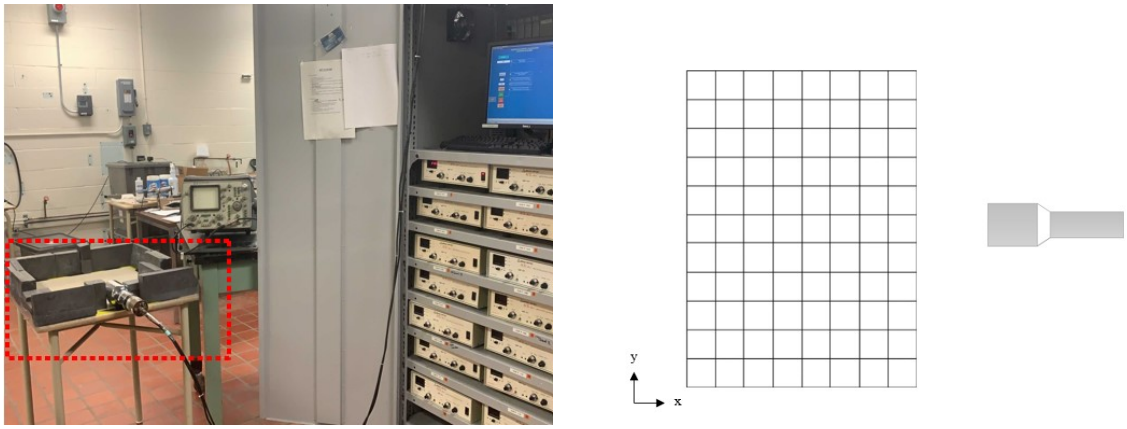

(a) Experimental RPT system

(b) Pattern used for recording the photon counts

Figure 2: Experimental setup for validation of optimization strategy

Figure 3a illustrates the experimentally measured and the predicted counts at several points on a straight line perpendicular to the detector face (one-dimensional validation). All the parameters optimized by NOMAD used in calculating the predicted photon counts are given in Table 3. Figure 3b shows a parity plot of the calculated photon counts by Lethe-RPT and the measured photon counts. The simulated data are in agreement with the measurements, which indicates the validation of the NOMAD blackbox optimizer in tuning the detector parameter using one-dimensional experimental data.

Table 3: Tuned parameters by NOMAD for 1D experiment

Parameter	Value
Detector dead time	$1.42 \times 10^{-5}\,\mathrm{s}$
Tracer activity	$2.35 \times 10^{6}\,\mathrm{Bq}$
μ_r	$9.88e-5$

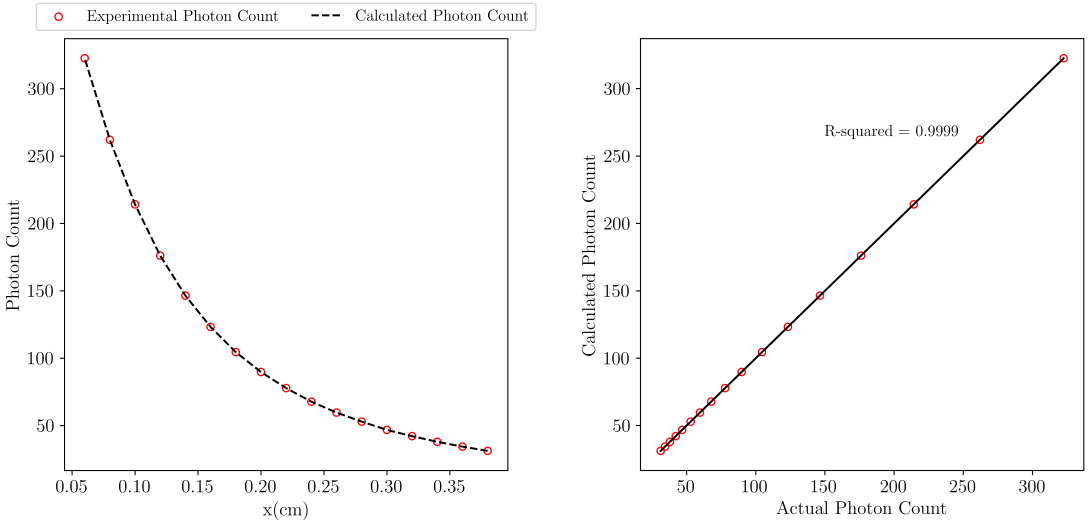

(a) Predicted and measured counts comparison

(b) Parity plot of the predicted and measured counts

Figure 3: 1D validation of optimization strategy

For a two-dimensional assessment of the algorithm the received photon counts by the detector from 108 points, and their associated positions feed the algorithm. Table 4 displays the results of the 2-dimensional detector's parameter tuning procedure. Figure 4 illustrates the parity plot of the calculated count using the optimized parameters and the experimentally measured counts. The 5% and -5% limits are also displayed in the figure. The simulated counts correspond well with the measured counts. The maximum deviation was about 2%, and the minimum was less than 1%. This indicates the validation of the Lethe-RPT code to calculate counts received by the detectors in the RPT calibration process.

Table 4: Tuned parameters by NOMAD for 2D experiment

Parameter	Value
Detector dead time	$9.74 \times 10^{-6}\,\mathrm{s}$
Tracer activity	$7.39 \times 10^{6}\,\mathrm{Bq}$
μ_r	0.457388

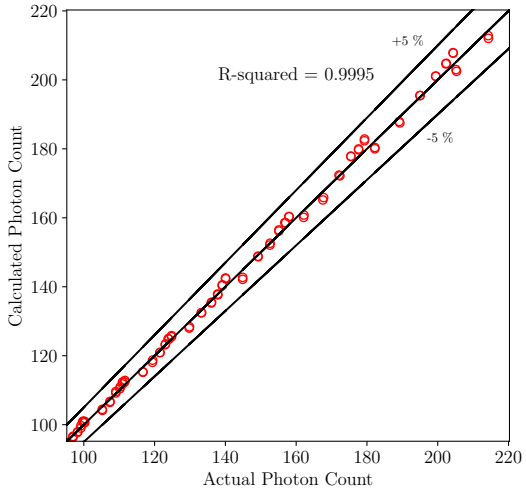

Figure 4: 2-D validation of optimization strategy

3.2. FEM-PR for position reconstruction

3.2.1. Theoretical study and sensitivity analysis

We carry out sensitivity analysis to evaluate the impact of the number of Monte Carlo iterations and number of cells on the accuracy of the FEM-PR algorithm. This virtual test determines the inherent error of the method independent of the experimental noise. The geometry is a cylinder with a 0.02 m radius and a 0.1 m height surrounded by six detectors, Figure 5 shows the detector configuration around the cylinder. We skip the calibration step and take default values for the three unknown parameters considering that all the detectors have the same physical properties.

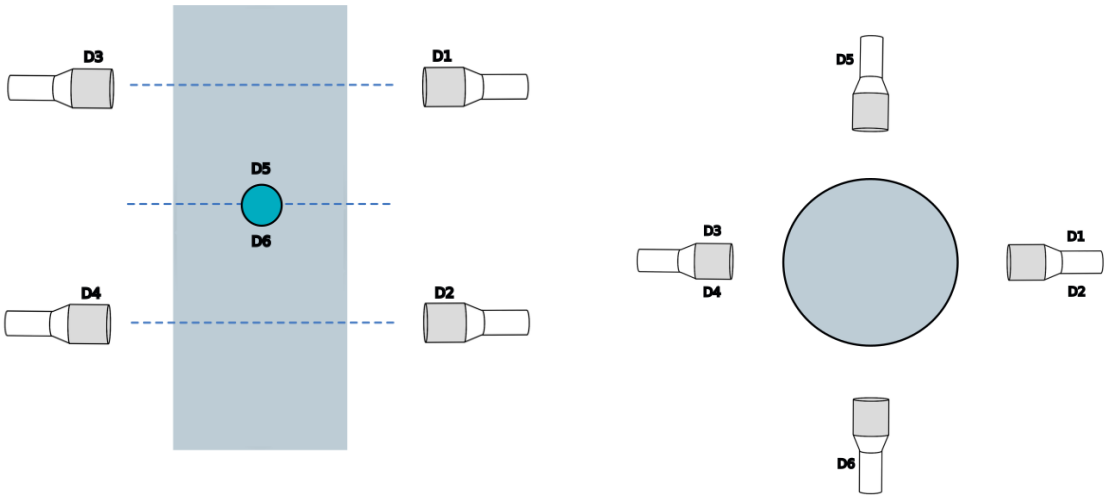

(a) Front view (b) Top view

Figure 5: RPT system simulated with Lethe-RPT

The mesh domain is generated through `deal.II` `GridGenerator` subdivided cylinder with tetrahedron elements [20]. We generated a spiral trajectory of 100 points and calculated the photon counts at each of the 6 detectors to verify FEM-PR's performance for 3D position reconstruction. Using the calculated photon counts, we reconstructed their positions. The algorithm was evaluated for 28 cases, which consisted of 7 mesh sizes and 4 different number of Monte Carlo iterations. We performed the simulations with different meshes ranging from 1920 to 30720 cells. We use performance indices such as Mean Absolute Error (MAE), Standard Deviation (SD), and Mean Euclidean Distance Error (MEDE) to assess the accuracy of the FEM-PR algorithm on the spiral trajectory. Figure 6a illustrates two key points:

- A sharp drop in error by increasing the number of cells from 3840 to 7680: the coarser meshes do not accurately represent the original geometry since they approximate curved boundaries using linear elements. Consequently, points close to the wall fall outside the mesh, making

it difficult to reconstruct their location. Refining the mesh allows us to fit the boundary and avoid reconstructing positions outside it. Because of this, there is a drop in reconstruction error by increasing the number of cells from 3840 to 7680.

- At a Monte Carlo iteration of 1000, which has the highest relative error in photon counts calculation (see Fig. 6b), refining the mesh results in a slight improvement in the algorithm performance. In contrast, at higher numbers of Monte Carlo iterations, more levels of refinement considerably decrease the error. In the first case, when the error of the Beam model (see Eq. 1) is high, all the points that the $\mathcal{L}^2$ projection uses for estimating the nodal count are also contaminated to a significant amount of error. Therefore, mesh refinement and increasing the available data points for the $\mathcal{L}^2$ projection does not filter the stochastic error of the Monte Carlo model and the reconstruction remains inaccurate. Conversely, at higher Monte Carlo iterations, when the data points in the domain are less impacted by the stochastic nature of Monte Carlo technique in the Beam model, and in fact, they are a valid representation of γ-rays radiation, increasing the number of cells allows the $\mathcal{L}^2$ projection to cancel the noise at full capacity. Consequently, searching through a clean data set reduces reconstruction error.

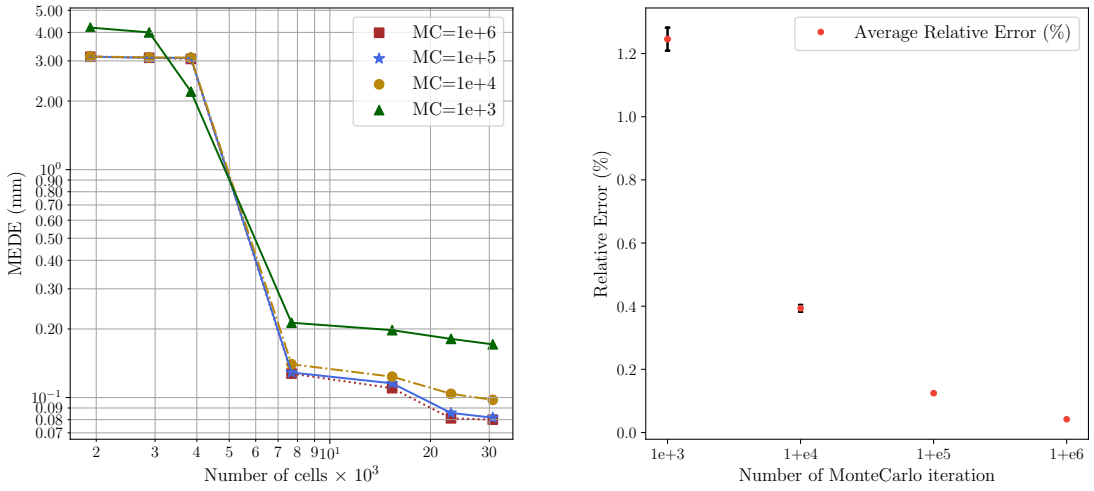

(a) (b)

Figure 6: (a) Comparison of MEDE and its dependency on cell numbers and Monte Carlo iterations for the spiral trajectory reconstruction; (b) Evaluation of error confidence interval for photon count generation regarding the number of Monte Carlo iterations for 2865 points inside the geometry

Values in Table 5 are the performance indices of the spiral trajectory reconstruction using Monte Carlo iterations equal to $1 + e6$. These data show a higher and more uneven error distribution for a coarser mesh. Figure 7 visualizes the spiral trajectory in XY and XZ planes.

The required computational time for reconstructing one position is around 3.37 ms, it is lower than the sampling time of the RPT hardware, 10 ms, which shows the capability of the FEM-PR algorithm for real time position reconstruction. This time does not include the detector parameter tuning and $\mathcal{L}_2$ orthogonal projection of the Monte Carlo model since they must be done before running the experiment.

Table 5: Reconstruction performance indices for $1 + e6$ Monte Carlo iteration

	MAE (mm)			SD (mm)			
Number of cells	X	Y	Z	X	Y	Z	MAED (mm)
1920	0.4	0.48	3	2.2	2.5	16.7	3.13
2880	0.29	0.52	3	1.9	2.9	16.7	3.1
3840	0.4	0.46	3	2.2	2.5	16.7	3.06
7680	0.04	0.06	0.09	0.08	0.13	0.06	0.13
15360	0.03	0.04	0.07	0.03	0.04	0.07	0.11
23040	0.02	0.04	0.06	0.02	0.04	0.05	0.08
30720	0.02	0.04	0.05	0.02	0.04	0 .04	0.08

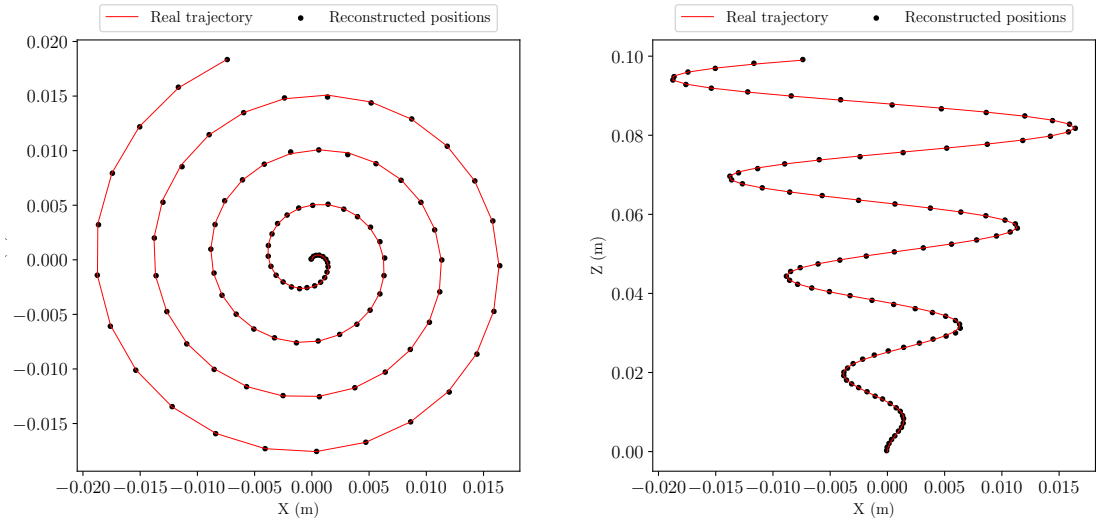

(a) XY plane

(b) XZ plane

Figure 7: Trajectory of the radioactive particle

3.2.2. Assessment and validation of the reconstruction algorithm

Finally, we assess the validity of the reconstruction algorithm with a reconstruction of a set of experimental points. The RPT system to check the validity of the proposed reconstruction algorithm consists of a square with dimensions of 0.12×0.12 m. We used a sealed Sc-46 tracer with a size of approximately 3 mm. We placed four (2" $\times$ 2") NaI scintillation detectors around the plane to

monitor the γ-rays radiation. The detectors were in one plane perpendicular to the z-axis and the distance between the detectors and the center of the plane was $0.24\,\mathrm{m}$. The photon count recorded by all detectors was saved on a computer through a data acquisition interface. The acquisition time at each position was 10 ms (data acquisition frequency of 100 Hz). We performed the calibration at 169 different locations. The registered counts of each of the four detectors, and their associated positions are the inputs of the detector's optimization algorithm. Using the tuned parameters for each detector we generate the dictionary for the corresponding geometry.

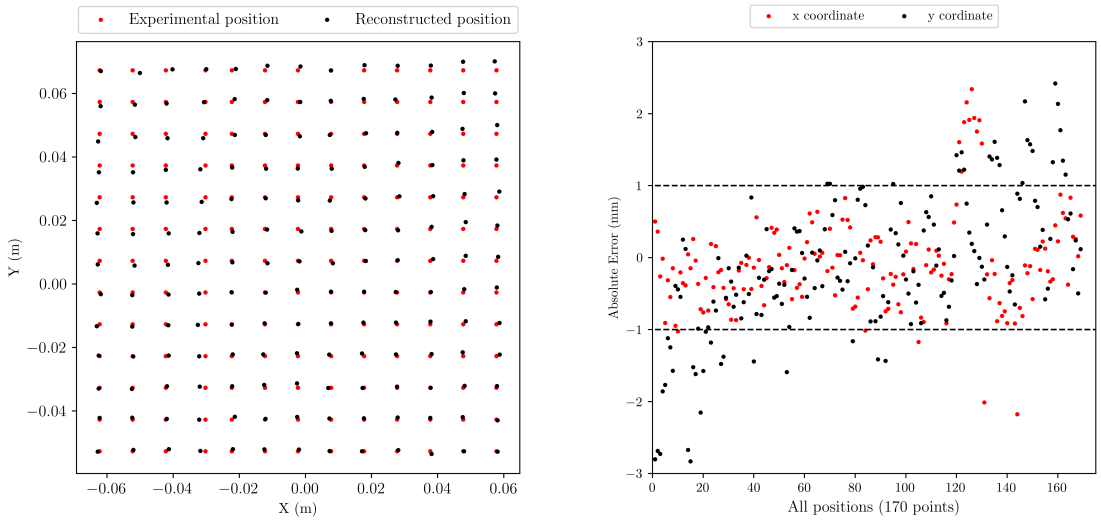

(a) Predicted and actual positions

(b) Absolute error

Figure 8: Predicted and actual positions error

Figure 8b shows the absolute error in predicting x and y coordinates over the entire dataset, and Figure 9 shows the parity plot of experimental and calculated coordinates for each point. The coefficient of determination (R^2) is 0.9997 for the x coordinate and 0.9993 for the y coordinate. The MAE error observed in x and y is 0.49 and 0.76 mm, with standard deviations of 0.68 and 0.98 mm, respectively. Figure 8a compares positions (x,y) predicted by Lethe-RPT and measured by experiment. According to these results, the algorithm can reconstruct the position with excellent

precision, which is better than the error reported by Yadav *et al.* (1.45 and 1.41 mm in x and y coordinates) [2].

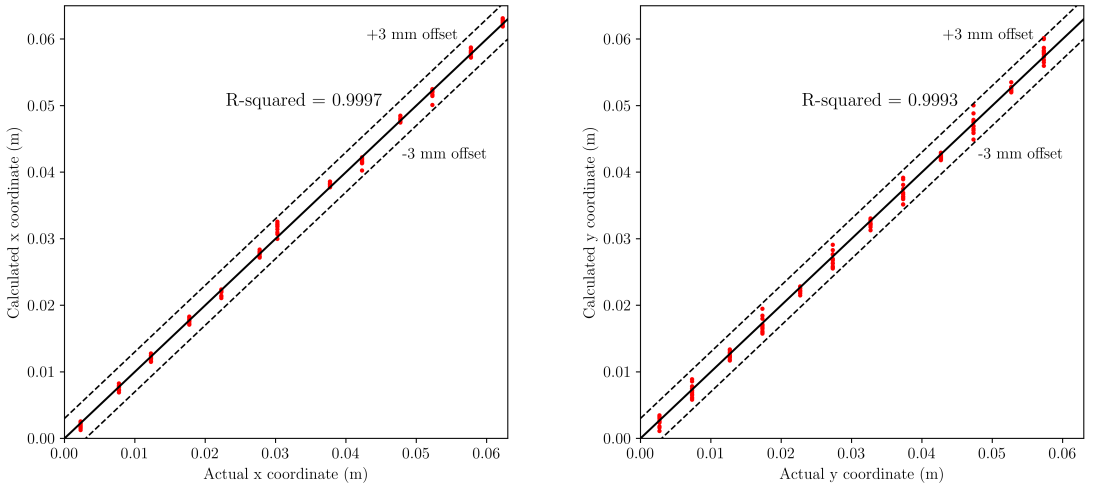

(a) Parity plot of predicted and experimental x coordinate

(b) Parity plot of predicted and experimental y coordinate

Figure 9: Parity plot of the predicted and experimental x and y coordinate

4. Conclusion

This paper presented a novel technique for reconstructing RPT experiments. We first presented a method to improve the model parameter optimization using a non-gradient based optimization algorithm. We then presented a reconstruction method using an inverse finite element method to retrieve the tracer's position using the model output.

We integrated the NOMAD blackbox optimization software into Lethe-RPT to calibrate the detector parameters. The entangled performance of the Monte Carlo engine and NOMAD optimizer for tuning the detector parameters was experimentally verified.

We compared the performance of the FEM-PR algorithm for various case studies in a "virtual" cylinder. An analysis of the sensitivity of simulation parameters, such as number of Monte Carlo

iterations and number of cells inside the meshed geometry, was presented. Using the mean Euclidean distance between the reconstructed tracer positions and the original ones, we determined the accuracy of the proposed technique. Our result indicates that the accuracy of the reconstruction increases as the number of Monte Carlo iterations and the number of cells in the mesh increase. Using a square surrounded by four detectors, we experimentally validated the FEM-PR approach accuracy by reconstructing tracer positions in two dimensions. We reconstructed the tracer position using a high number of Monte Carlo iterations to as much as possible minimize the inherent error of the model for photon count calculations. A combination of a high number of Monte Carlo iterations and a high number of cells inside the mesh enables the FEM-PR to eliminate Monte Carlo noise and provides smooth data sets of photon counts. Therefore, the algorithm searches through a clean dataset and finds the unique cell that meets the condition of the inverse finite element method. FEM-PR drastically reduces the reconstruction error, it reconstructs the position with an accuracy of 0.08 mm. Additionally, FEM-PR is a promising method for real time position reconstruction since the computational time is less than the sampling time of the traced photons from the radioactive source.

The applicability of this reconstruction algorithm is not limited to RPT as it could be readily extended to other fields in which inverse reconstruction problems have to be solved, such as medical imaging techniques, shape sensing for structural deformation, reconstruction of the sound pressure field, and other particle tracking techniques like Positron Emission Particle Tracking (PEPT).

5. Acknowledgements

Ghazaleh Mirakhori would like to acknowledge the support received from Dr. Rouzbeh Jafari and Dr. Hamed Nasri. The authors would like to acknowledge the financial support from the Natural Sciences and Engineering Research Council of Canada (NSERC) through the NSERC CRDPJ 536981-1 grant. The authors would also like to acknowledge technical support and computing time

provided by the Digital Research Alliance of Canada and Calcul Québec.

References

[1] R. K. Upadhyay, H. J. Pant, S. Roy, Experimental validation of design and performance parameters of radioactive particle tracking (rpt) experimentation, Applied Radiation and Isotopes 153 (2019) 108814.

[2] A. Yadav, T. K. Gaurav, H. J. Pant, S. Roy, Machine learning based position-rendering algorithms for radioactive particle tracking experimentation, AIChE Journal 66 (6) (2020) e16954.

[3] J. Chaouki, F. Larachi, M. Dudukovic, Non-invasive monitoring of multiphase flows, Elsevier, 1997.

[4] R. K. Upadhyay, Investigation of multiphase reactors using radioactive particle tracking, Ph.D. thesis (2010).

[5] A. A. Alghamdi, T. M. Aljuwaya, A. S. Alomari, M. H. Al-Dahhan, Geant4 simulation for radioactive particle tracking (rpt) technique, Sensors 22 (3) (2022) 1223.

[6] J. Chen, A. Kemoun, M. H. Al-Dahhan, M. P. Duduković, D. Lee, L.-S. Fan, Comparative hydrodynamics study in a bubble column using computer-automated radioactive particle tracking (carpt)/computed tomography (ct) and particle image velocimetry (piv), Chemical engineering science 54 (13-14) (1999) 2199–2207.

[7] A. Yadav, M. Ramteke, H. J. Pant, S. Roy, Monte carlo real coded genetic algorithm (mc-rga) for radioactive particle tracking (rpt) experimentation, AIChE Journal 63 (7) (2017) 2850–2863.

[8] A. Tessler, J. L. Spangler, A least-squares variational method for full-field reconstruction of elastic deformations in shear-deformable plates and shells, Computer methods in applied mechanics and engineering 194 (2-5) (2005) 327–339.

[9] B. Blais, L. Barbeau, V. Bibeau, S. Gauvin, T. El Geitani, S. Golshan, R. Kamble, G. Mirakhori, J. Chaouki, Lethe: An open-source parallel high-order adaptative cfd solver for incompressible flows, SoftwareX 12 (2020) 100579.

[10] G. Beam, L. Wielopolski, R. Gardner, K. Verghese, Monte carlo calculation of efficiencies of right-circular cylindrical nai detectors for arbitrarily located point sources, Nuclear instruments and methods 154 (3) (1978) 501–508.

[11] M. Rasouli, F. Bertrand, J. Chaouki, A multiple radioactive particle tracking technique to investigate particulate flows, AIChE Journal 61 (2) (2015) 384–394.

[12] F. Larachi, G. Kennedy, J. Chaouki, A γ-ray detection system for 3-d particle tracking in multiphase reactors, Nuclear Instruments and Methods in Physics Research Section A: Accelerators, Spectrometers, Detectors and Associated Equipment 338 (2-3) (1994) 568–576.

[13] L. Godfroy, F. Larachi, G. Kennedy, B. Grandjean, J. Chaouki, On-line flow visualization in multiphase reactors using neural networks, Applied Radiation and Isotopes 48 (2) (1997) 225–235.

[14] C. Audet, S. Le Digabel, V. Rochon Montplaisir, C. Tribes, NOMAD version 4: Nonlinear optimization with the MADS algorithm, Tech. Rep. G-2021-23, Les cahiers du GERAD (2021).
URL http://www.optimization-online.org/DB_HTML/2021/04/8351.html

[15] C. Audet, W. Hare, Derivative-free and blackbox optimization, Vol. 2, Springer, 2017.

[16] C. Audet, J. E. Dennis Jr, Mesh adaptive direct search algorithms for constrained optimization, SIAM Journal on optimization 17 (1) (2006) 188–217.

[17] O. Dubé, D. Dubé, J. Chaouki, F. Bertrand, Optimization of detector positioning in the radioactive particle tracking technique, Applied Radiation and Isotopes 89 (2014) 109–124.

[18] C. A. Felippa, Introduction to finite element methods, University of Colorado 885 (2004).

[19] M. G. Larson, F. Bengzon, The finite element method: theory, implementation, and applications, Vol. 10, Springer Science & Business Media, 2013.

[20] D. Arndt, W. Bangerth, M. Feder, M. Fehling, R. Gassmöller, T. Heister, L. Heltai, M. Kronbichler, M. Maier, P. Munch, J.-P. Pelteret, S. Sticko, B. Turcksin, D. Wells, The `deal.II` library, version 9.4, Journal of Numerical Mathematics 30 (3) (2022) 231–246. `doi:10.1515/jnma-2022-0054`.
URL `https://dealii.org/deal94-preprint.pdf`